Low-energy H^+, He^+, N^+, O^+, and Ne^+ scattering from metal and ionic-compound surfaces: Neutralization and electronic excitation

R. Souda, K. Yamamoto, W. Hayami, T. Aizawa, and Y. Ishizawa
National Institute for Research in Inorganic Materials, 1-1 Namiki, Tsukuba, Ibaraki 305, Japan
(Received 12 September 1994)

Neutralization and electronic excitation during low-energy ion-surface scattering have been investigated from a combination of experiments and molecular-orbital energy calculations based on the discrete variational $X\alpha$ method. It is found that a variety of electronic transitions are mediated by the molecular orbitals during the violent collision or the short-lived chemisorption state of the ions, which may not be inferred from the atomic orbitals of the isolated projectiles. The rare-gas ions, such as He^+ and Ne^+, capture a valence electron mainly via the Auger neutralization process, whereas resonant tunneling can also play an important role in neutralization of the reactive ions (H^+, N^+, O^+). The occurrence of resonant tunneling is related to the open-shell structure of the reactive ions. The probability for resonance neutralization is sensitively dependent upon the nature of the valence band (band effect) and is largely enhanced at the metal surface relative to the ionic-compound surface. The valence-band electron can be excited in scattering of reactive ions as a sequence of neutralization/ionization along the promoted antibonding molecular orbital. In scattering of the rare-gas ions, not only the valence electron but also the semicore electron can be excited for specific ion-target combinations in which sufficient promotion of the antibonding molecular orbital can take place during collision.

I. INTRODUCTION

Charge exchange between particles and solid surfaces has attracted considerable attention from fundamental as well as practical points of view. A better understanding of the charge-exchange phenomena is of essential importance as the basis of surface analysis techniques using ions, such as low-energy ion scattering (LEIS), secondary-ion-mass spectroscopy (SIMS), and electron-stimulated desorption (ESD). In terms of ion neutralization, it is a generally held belief that a valence electron is captured via resonance neutralization (RN) and/or Auger neutralization (AN), and that the relative role of these processes is determined by the energy position of the vacant ionic level relative to the valence band.[1] On the other hand, there are some indications that the ion-surface charge exchange has a more local character than expected from the electron-gas model, and is dependent much more sensitively upon the species of the target atoms.[2] This is in fact the case for backscattering events, in which a violent collision between incoming and outgoing trajectories may play an important role in determining the final charge state of the projectile. Two of the well-known examples are the occurrence of reionization[2] and the production of doubly excited autoionizing states.[3] These processes are essentially the same in origin and are caused by the electron promotion mechanism.[4,5]

So far, considerable research effort has been devoted to alkali-metal ions and rare-gas ions, but a few investigations had been made of the other ions which might be classified as reactive ions. The interactions of reactive ions with surfaces are seemingly quite different from those of the rare-gas ions. For example, the neutralization probability of H^+ is quite large compared to He^+, and the surface peaks, which originate from ions scattered from the topmost-layer atoms without neutralization, are often completely absent at metal surfaces.[6] A valence electron should be captured via AN by both H^+ and He^+ ions since their $1s$ levels are located well below the valence-band top position. However, the large difference in neutralization probability between H^+ and He^+ may not be elucidated only by AN. We have suggested that the large neutralization probability of H^+ is due to the additional contribution of RN and, hence, the neutralization probability is closely related to the valence-band structure of a surface (band effect).[7,8] This assumption has recently been confirmed from molecular-orbital (MO) energy calculations of H^+ interacting with various surface clusters.[9] In this paper, the mechanism of neutralization and electronic excitation of H^+, He^+, N^+, O^+, and Ne^+ ions scattered from Pt(111), $SrTiO_3$(001), and CsBr surfaces will be investigated from a combination of experiments and MO energy calculations.

II. EXPERIMENT

The experiments were made in an ultrahigh vacuum chamber equipped with facilities for LEIS, ultraviolet photoelectron spectroscopy, low-energy electron diffraction (LEED), and a load-lock system for sample transfer. Ions were generated in a discharge-type ion source and were mass analyzed by using a Wien filter. Ions with kinetic energy E_0 ranging from 10 eV to 1 keV could be incident upon a surface with an angle of 80° from the surface, and ions scattered through a laboratory scattering angle of 160° were detected by means of a hemispherical electrostatic energy analyzer operating with a constant energy resolution of 1 eV.

The Pt(111) surface was prepared with a standard oxygen treatment, and showed an excellent 1×1 pattern in

LEED. The $SrTiO_3(001)$ surface was cleaned by repeated sputtering/annealing cycles. A thin film of polycrystalline CsBr was evaporated *in situ* on a substrate of pyrolytic graphite. The samples of Pt(111) and $SrTiO_3(001)$ were mounted on a tandem sample holder, so that the backscattered ion intensities could be compared relative to each other under the condition of the same ion-beam flux.

III. EXPERIMENTAL RESULTS

Figure 1 shows the energy spectra of $E_0=500$-eV H^+ ions scattered from (a) the $SrTiO_3(001)$ surface and (b) the Pt(111) surface. The intensities are normalized through the beam current. The arrows on the abscissa indicate the positions of the elastic binary-collision energy (BCE) for individual target atoms. Sharp peaks appearing at around the BCE of Sr and O in Fig. 1(a) are the surface peaks which come from H^+ surviving neutralization in a single collision with the topmost-layer atoms, whereas the surface peak of Ti is not remarkable. The surface peak is absent at the Pt(111) surface, and the spectrum is composed mainly of a broad background which originates from the H^+ ions ejected from the surface after penetration into the deeper layers. The background has been assigned to reionization ($H^+ \rightarrow H^0 \rightarrow H^+$) of neutralized H^+ which occurs in a collision with the topmost-layer atoms just before leaving the surface.[7] Here the background will not be discussed in detail, and attention is mainly focused on the structure and intensity of the surface peaks of Sr at $SrTiO_3(001)$ and Pt at Pt(111). The surface peak of Sr in Fig. 1(a) is composed not only of the elastic peak *A* but also of the energy-loss peak labeled *B*. Peak *B* has been attributed to *e-h* pair excitation because of the good correlation between its energy-loss value and the band-gap energy of the surface.[7]

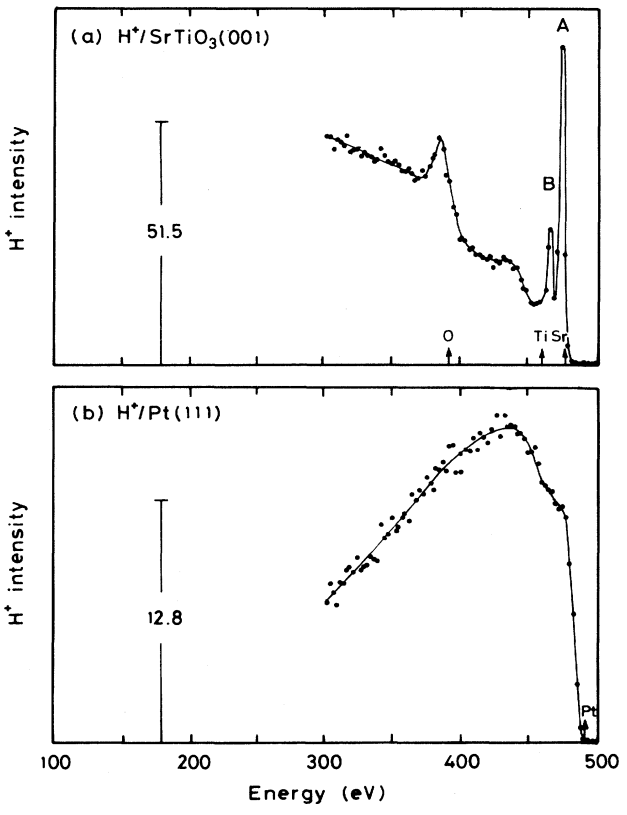

FIG. 1. Energy spectra of $E_0=500$ eV H^+ ions scattered from (a) the $SrTiO_3(001)$ surface and (b) the Pt(111) surface. The measurements were made with a scattering angle of 160° and a glancing angle of 80°. The intensities are normalized relative to each other through beam current. The energies corresponding to elastic binary collisions with individual target atoms are indicated by arrows with chemical symbols on the abscissa.

Shown in Fig. 2 is the energy spectrum of $E_0=500$-eV He^+ scattered from (a) $SrTiO_3(001)$ and (b) Pt(111). The Sr peak is composed of three peaks *A*, *B*, and *C*.[7] Peak *B* is due to *e-h* pair excitation similar to that in the H^+ spectrum, while peak *C* is characteristic of He^+-Sr collision and is assignable to reionization ($He^+ \rightarrow He^0 \rightarrow He^+$) or excitation of the Sr 4*p* semicore electron. At the Pt(111) surface, the Pt peak is remarkable and the background is almost absent, which is in sharp contrast to the results of H^+ scattering shown in Fig. 1(b). Although the spectral intensities are normal-

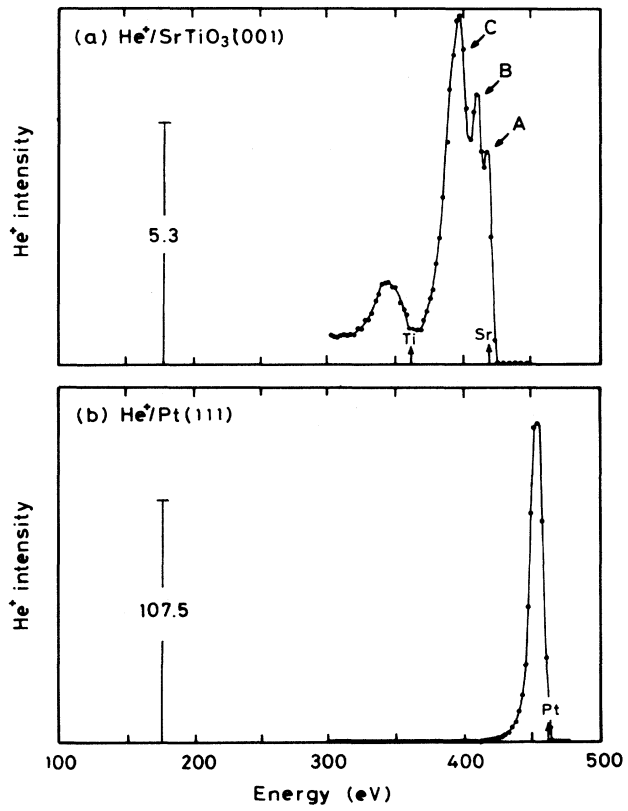

FIG. 2. Energy spectra of $E_0=500$ eV He^+ ions scattered from (a) the $SrTiO_3(001)$ surface and (b) the Pt(111) surface. The measurements were made under the same conditions as in Fig. 1. The intensities are normalized relative to each other through the beam current.

ized through the beam current, no correction of the secondary particle emission is made for different ion-beam impact. So the indicated intensity may be somewhat a rough measure. Despite these uncertainties, the observed contrast in the appearance of the Pt peak between H^+ and He^+ scattering is remarkable and might be related to the difference in the 1*s* orbital energy position between H (-13.6 eV) and He (-24.6 eV).

The nature of charge exchange of N^+, O^+, and Ne^+ may be different from that of H^+ and He^+ since the ionic orbitals relevant to neutralization are different between these two kinds of projectiles (2*p* for the former and 1*s* for the latter). The energy spectra of N^+, O^+, and Ne^+ ions scattered from (a) $SrTiO_3(001)$ and (b) Pt(111) are displayed in Figs. 3–5. Although the Pt peak intensity is larger than the Sr peak intensity in Ne^+ scattering, the contrary is true for N^+ and O^+ scattering. The surface peak is composed of a broad, single peak in N^+ and O^+ scattering, and its position is apparently lower than the BCE of Sr and Pt, indicating the occurrence of the inelastic energy loss. The structures of the Sr peak shown in Figs. 3 and 4 are unchanged even if the ion energy is decreased to 200 eV, below which the surface peak becomes too small to be detected.

In N^+ and O^+ scattering from CsBr, on the other hand, the surface peak intensity is not so decreased with decrease of E_0 and its structure is changed dramatically. The typical results for O^+ scattering are shown in Fig. 6. The Cs and Br peaks at $E_0=500$ eV are broad compared to the Sr peak shown in Fig. 4(a). The Cs peak is composed not only of the energy-loss peak (peak *B*) but also of elastic peak *A*, as seen in Figs. 6(b)–6(d), where the intensity of peak *B* is decreased with a decrease of the energy and peak *A* becomes a main peak if E_0 goes below 200 eV.

IV. DISCUSSION

The projectile ions examined here can readily be classified into two groups: One is the rare-gas ions (He^+,Ne^+) for which the Pt peak intensity is comparable to or larger than the Sr peak intensity. The other is the reactive ions (H^+, N^+, O^+) which are characterized by the extremely small intensity of the Pt peak and the relatively large Sr peak. The rare-gas ions, having an ionic level well separated from the valence band, capture a valence electron mainly via the AN process, and no marked target-element dependencies of the neutralization probability may occur. For reactive ions, on the other

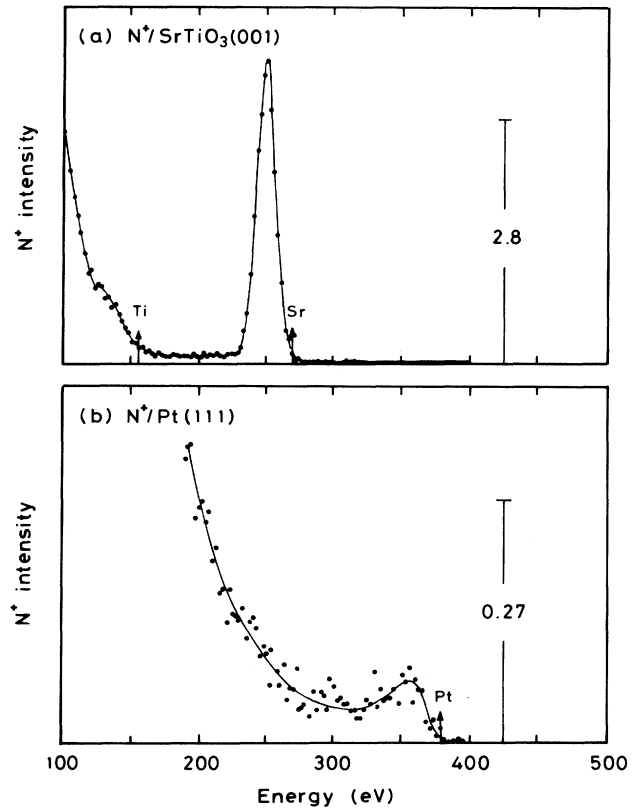

FIG. 3. Energy spectra of $E_0=500$ eV N^+ ions scattered from (a) the $SrTiO_3(001)$ surface and (b) the Pt(111) surface. The measurements were made under the same conditions as in Fig. 1. The intensities are normalized relative to each other through the beam current.

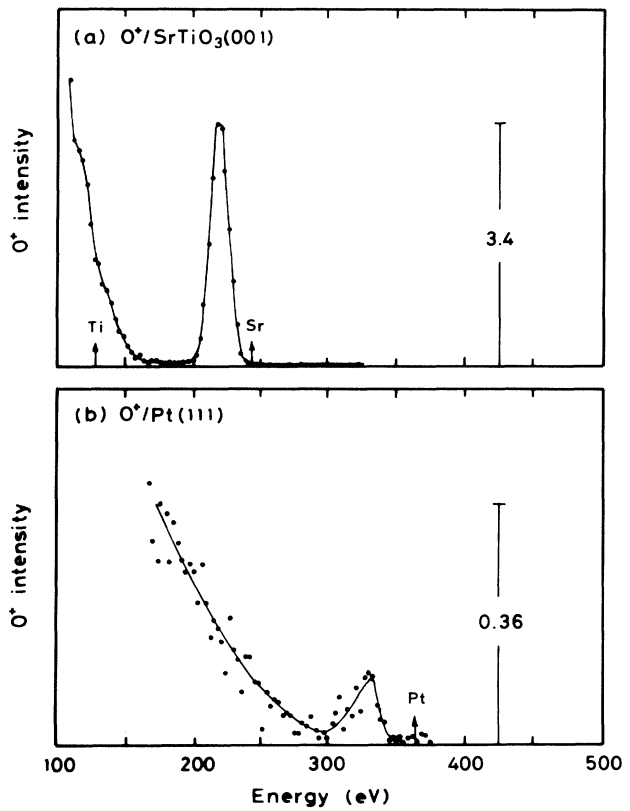

FIG. 4. Energy spectra of $E_0=500$ eV O^+ ions scattered from (a) the $SrTiO_3(001)$ surface and (b) the Pt(111) surface. The measurements were made under the same condition as in Fig. 1. The intensities are normalized relative to each other through the beam current.

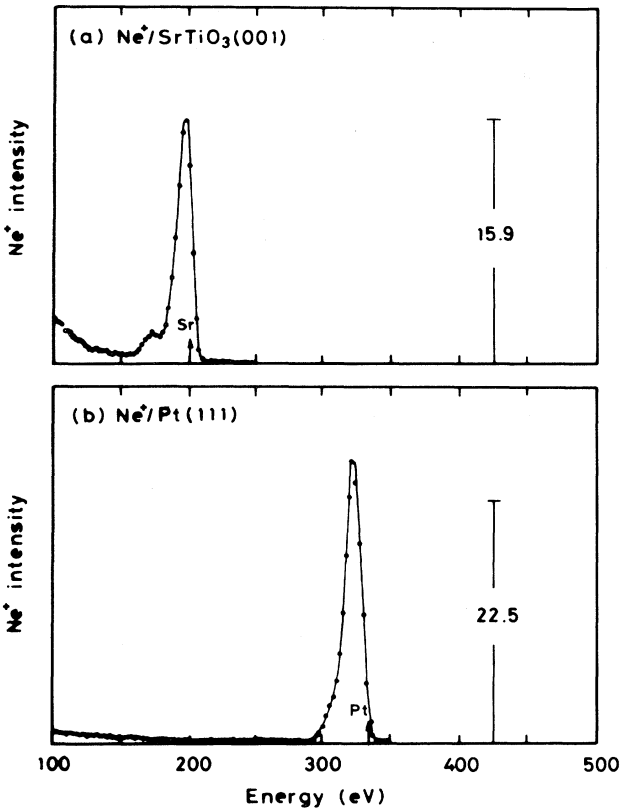

FIG. 5. Energy spectra of $E_0=500$ eV Ne^+ ions scattered form (a) the $SrTiO_3(001)$ surface and (b) the Pt(111) surface. The measurements were made under the same conditions as in Fig. 1. The intensities are normalized relative to each other through the beam current.

hand, the neutralization probability seems correlated to the ionicity of the target atoms (Pt,Sr^{2+}), which may not be explained only by AN. In the particular case of D^+ scattering, it is suggested that RN can play an important role because the D 1*s* level may possibly resonate with the valence band due to the image-charge effect.[7,8]

So far, ion neutralization has been described on the basis of the band picture combined with the atomic orbital (AO) of the projectile which is modified due to the interaction with the surface. This scheme concludes the occurrence of AN for all of the ions discussed here, since their ionic levels are deep enough relative to the valence-band top position. Indeed, this is confirmed experimentally from the detection of Auger electrons by ion-beam impact.[10,11] The concept of the AO should be valid when the ions are located far from the surface [$d>4-5$ atomic unit (a.u.)], but the charge-exchange phenomena, occurring in both close encounters and surface regions over which the projectile is in strong, chemisorption-type, interaction with the surface, should be much better described by MO's than by AO's. AO's merge into MO's continuously with a decrease of the distance. To our knowledge, however, there is no theory that can describe this transient region precisely. One convincing way is to extrapolate the current treatment of the broadening and shift of the AO to smaller encounters, so that its behavior corresponds to MO's. It is also depicted that the neutralization probability is sensitively dependent upon the nature of the valence band if the RN condition is satisfied (band effect).[12] This is true for both AO- and MO-based pictures, and of importance is the energy position of the projectile-derived state relative to the valence band. These points are indeed essential for neutralization of the reactive ions since the ionic level hybridizes preferentially with the valence band, as will be shown below. In any case, the closer the ion approaches the surface, the greater the transition rate of the valence electron. Therefore, knowledge of the MO energy of the colliding complex is crucial for describing the ion-surface charge-exchange phenomena precisely.

The MO energy-level diagram is numerically calculated with the use of the self-consistent-charge discrete variational $X\alpha$ (SCC-DV-$X\alpha$) method; the strategy of the calculation has been shown elsewhere.[13,14] Briefly, the Hartree-Fock-Slater (HFS) equation for a cluster is solved self-consistently with the use of a localized exchange potential ($X\alpha$ potential). The exchange-correlation parameter α is adjustable and is taken as 0.7. Numerical atomic orbitals, obtained as solutions of the atomic HFS equations, were used as basis sets. To simulate scattering of X^+ ions from Sr^{2+} of $SrTiO_3(001)$ and Cs^+ of CsBr(001), the calculations are made by using $(XSrO_5)^{7-}$ and $(XCsBr_5)^{3-}$ clusters, in which 1*s*, 2*s*, and 2*p* orbitals are commonly used for X^+. For X^+ scattering from Pt(111), the calculations are made by using a diatomic molecule, $(XPt)^+$.

A. H^+ and He^+

The calculated MO energy of the $(HSrO_5)^{7-}$ cluster is displayed in Fig. 7. The results are plotted so that the energy-level position of MO's with the H 1*s* component can be surveyed as a function of the distance *d* of the ions from the target Sr atom; the population of the H 1*s* atomic-orbital component in each MO is indicated by the length of the horizontal bar. The orbital character changes as a function of the distance, and the typical dominant character at $d=5.0$ a.u. is shown in the figure. The energy of the valence-band top (or the highest occupied molecular orbital: HOMO) position is arbitrarily set at zero. The distance of the closest approach for $E_0=500$-eV H^+ on Sr is indicated by an arrow on the abscissa.

The H 1*s* orbital is hybridized with the valence-band orbitals ($13-16a_1$), indicating the formation of the bound state. This result shows that RN does occur between H 1*s* and the valence band. The exception is the close encounter ($d<1.5$ a.u.), where the major portion of H 1*s* is transferred to $16-20a_1$ orbitals (the antibonding orbital) and the $10a_1$ and $9a_1$ orbitals (the bonding orbitals). Adiabatic MO's with the same symmetry avoid crossing, but the variation of the H 1*s* component in the $16-20a_1$ orbitals gives diabatic MO's. The occurrence of electronic excitation necessitates diabatic electron transition at the (pseudo) crossing point of the calculated adiabatic MO's. The promotion of the diabatic MO is essentially caused by the Pauli repulsion due to penetration of H 1*s*

into the Sr 4*s* and 4*p* closed-shell orbitals, as evidenced by the hybridization of H 1*s* and the corresponding atomic orbitals.

The promotion of the diabatic MO shown in Fig. 7 is responsible for the *e-h* pair excitation resulting in peak *B* of Sr: The valence electron can be excited along the diabatic MO if the electron is captured via AN or RN on the incoming trajectory. This is followed by resonance ionization (RI) due to electron diffusion into the empty conduction-band states. If the resultant ions survive neutralization on the outgoing trajectory, they finally form peak *B* in the energy spectra.

In Fig. 8 the MO energy-level diagram for He^+ on the $(SrO_5)^{8-}$ cluster is shown. In contrast to the H^+ scattering shown in Fig. 7, the He 1*s* character appears in $10a_1$, $11a_1$, and $13a_1$ orbitals at a large separation, and is not distributed in the valence-band orbitals. Therefore, He^+ captures a valence electron mainly via AN. With a decrease of the separation, the He 1*s* component is almost equally distributed in the bonding $10a_1$ orbital and the antibonding $13a_1$ orbital. This is characteristic of the He^+-Sr collision, and is caused by the hybridization of the closely located He 1*s* and Sr 4*p* orbitals. The antibonding $13a_1$ orbital is diabatically correlated to the $19a_1$ and $20a_1$ orbitals in a close encounter.

The crossing of the antibonding MO with the valence- or conduction-band states causes a variety of electronic transitions other than AN: Along the promoted MO, the electron of the He 1*s*, Sr 4*p*, and O 2*p* orbitals can be excited into the empty conduction-band state (the $19a_1$ and $20a_1$ orbitals). Indeed, the excitation of the valence electron (peak *B*) and the Sr 4*p* electron (peak *C*) is observed experimentally in Fig. 2(a). On the other hand, excitation of the He 1*s* electron is well known to occur as reionization,[2] in which He^+ is neutralized on the incoming trajectory via AN and is ionized due to electron excitation to the conduction-band state during the collision. In addition, the creation of the semicore holes either in the projectile or in the target results in the autoionizing state.[3] Thus electronic states shallower than the He 1*s* level can basically be excited due to hybridization of He 1*s* with the semicore orbital of the target, which is in sharp contrast to H^+ scattering, where only the shallowest valence electron can be excited. Furthermore, ion neutralization other than AN is mediated by MO's; the vacancy of the He 1*s* orbital can be transferred to the Sr 4*p* state or the valence-band state. They are classified as quasiresonant neutralization[15–17] (QRN; the Sr 4*p* final hole state) and collision-induced neutralization[18,19] (CIN; the O 2*p* final hole state).

The MO energies calculated for the $(HPt)^+$ molecule are shown in Fig. 9. The H 1*s* component is distributed over the valence-band orbitals; the 13σ and 14σ orbitals are caused by hybridization of H 1*s* with the Pt 5*d* state, and 15σ and 16σ have Pt 6*s* and 6*p* characters, respectively. In a close encounter ($d \sim 1$ a.u.), the antibonding

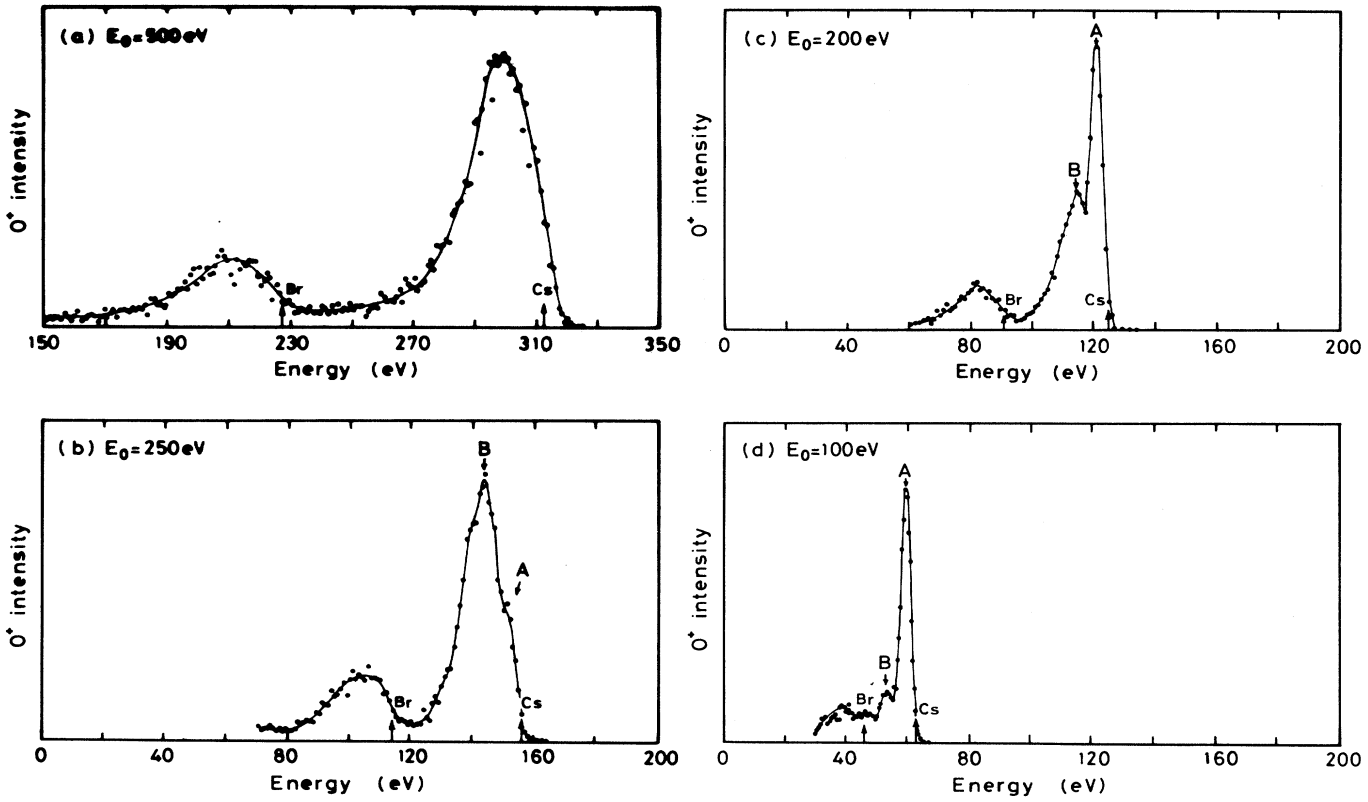

FIG. 6. Energy spectra of O^+ ions scattered from the polycrystalline CsBr surface. The measurements were made by changing the primary beam energy from 500 to 100 eV.

orbital ($16-18\sigma$) is highly promoted as a consequence of interaction with the Pt $5s$ and $5p$ semicore orbitals (not shown in Fig. 9). The calculation is also made with a larger cluster, $(HPt_{10})^+$. The results are similar to the case of the diatomic molecule shown here, except that the H $1s$ character is distributed in a larger number of the valence-band orbitals. The RN condition is thus found to be satisfied between H $1s$ and the valence band of the Pt(111) surface.

Shown in Fig. 10 are MO's of He^+ interacting with Pt. At a large separation, the 13σ orbital is composed mostly of the He $1s$ atomic orbital, and there is no He $1s$ component in the valence-band orbitals. Hence the He^+ ion captures the valence electron mainly via AN. The He $1s$ orbital (13σ) has a bonding character with no promotion, so that no significant electronic excitation is thought to occur. This is the reasons why the Pt peak shown in Fig. 2(b) is so large in intensity and exhibits no energy-loss structures.

From the above discussion, it is revealed that H^+ captures a valence electron via RN, whereas neutralization of He^+ occurs mainly via AN. It should be noted that the hybridization of H $1s$ with the valence band, or the occurrence of RN in H^+ scattering, is not simply related to the H $1s$ energy position closer to the valence band but is essentially caused by the open-shell structure of H $1s$. The equilibrium charge of the projectiles can be obtained from the Mulliken population analysis: He^+ and H^+ should be neutralized completely, though hydrogen can be charged slightly negatively. In real ion-scattering events, charge exchange is a highly dynamical process, and its probability is determined at least by two competitive factors. One is, of course, the duration of the ion-surface interaction, $T\sim10^{-15}$ sec, and the other is the transition rate ω of the valence electron. The experimental results at the Pt(111) surface shown in Figs. 1(b) and 2(b) are good cases to compare the transition rates of the valence electron between RN and AN. The absence (presence) of the Pt peak in H^+ (He^+) scattering at the Pt(111) surface indicates that the RN occurs much more efficiently than AN. The contrary occurs for the Sr peak at the $SrTiO_3$(001) surface, where the Sr peak is more remarkable in H^+ scattering than in He^+ scattering. This result can be elucidated on the basis of the band effect on the RN process as described below: The probability of RN is determined by the lifetime $\tau(=1/\omega)$ of the electron (or hole) in the valence band. τ is roughly estimated by using the valence-band width W as

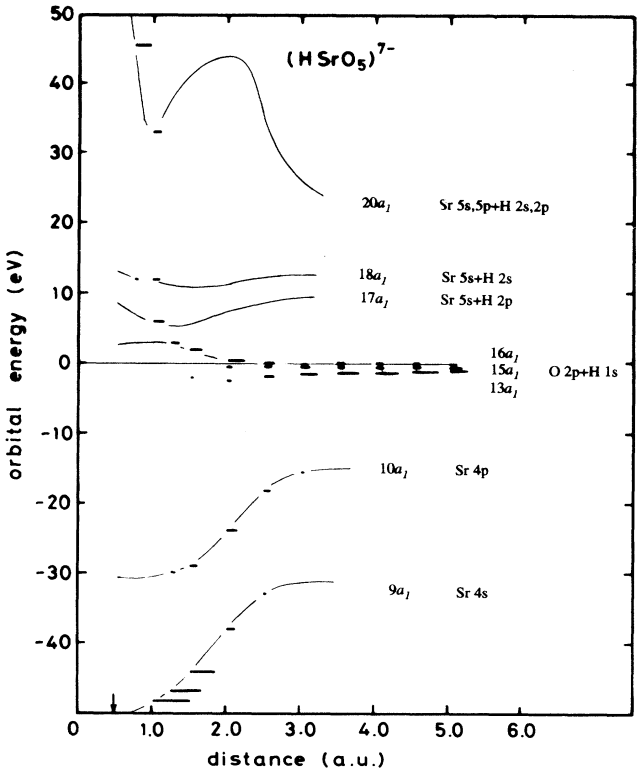

FIG. 7. Energy-level diagram of the $(HSrO_5)^{7-}$ cluster simulating H^+ scattering from Sr^{2+} of the $SrTiO_3$(001) surface. The energy of MO's with H $1s$ character is displayed as a function of the internuclear distance d, where the valence-band top position is arbitrarily set at zero. The length of the horizontal bar indicates the population of the H $1s$ atomic-orbital component in each MO. The orbital character changes as a function of the distance, and the dominant orbital character at $d=5.0$ a.u. is typically indicated. The distance of the closest approach for $E_0=500$ eV H^+ on Sr^{2+} is shown by an arrow on the abscissa.

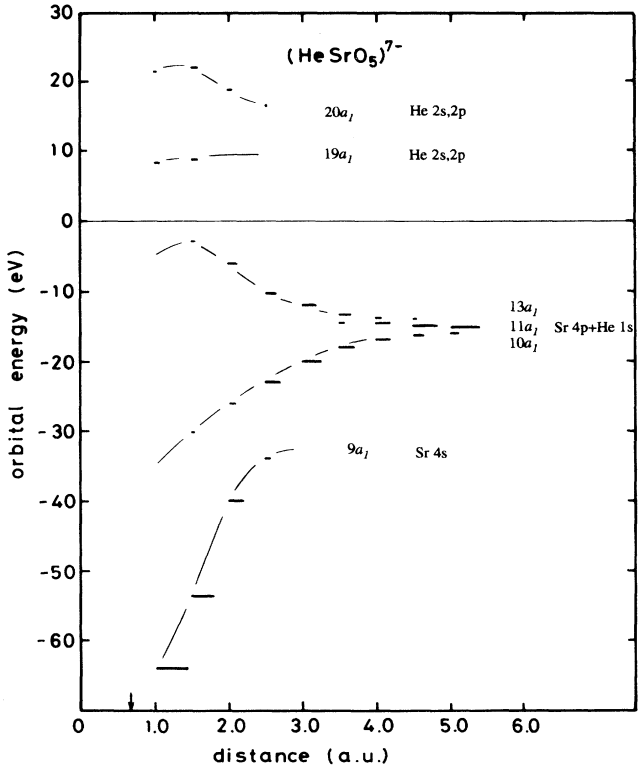

FIG. 8. Same as Fig. 7, but for the $(HeSrO_5)^{7-}$ cluster. The energy position and population of the He $1s$ component in the a_1 orbital are indicated by the horizontal bars.

$$\tau=\hbar/W \ . \tag{1}$$

The experimental fact that H^+ is almost completely neutralized at the Pt(111) surface shows that the equilibrium product (H^0 or H^-) is formed during scattering due to the large mobility of the valence electron, whereas the equilibration is difficult to occur in H^+ scattering from the $SrTiO_3(001)$ surface because of the narrow band width or the insufficient electron mobility. This situation reminds us of QRN of He^+,[15–17] where the He 1s hole is confined in the molecular orbital formed between H 1s and the semicore orbital of the target and cannot diffuse into the electronic states of the surrounding atoms. In these cases, the averaged neutralization probability is shown to be at most 0.5.[17]

From the Sr peak displayed in Fig. 1(a), we can roughly estimate the neutralization (AN and RN) probability as follows. Taking into account the fact that elastic peak A arises from survival of H^+ on both incoming and outgoing trajectories while peak B comes from H^+ which experienced a sequence of neutralization on the incoming trajectory, RI in collision, and survival of neutralization on the outgoing trajectory, we can give the intensity of peak B relative to peak A as

$$I_B/I_A=pf/(1-p) \ , \tag{2}$$

where p and f represent the probabilities for neutralization (AN+RN) and RI, respectively. If the electron is promoted sufficiently into the conduction-band state, we can put f at being close to unity. This assumption is ensured by the fact that the width of the conduction band is so large compared to the valence band that the lifetime of the electron in the conduction band should be small. Then I_B/I_A is given with a simpler form $p/(1-p)$. By using the experimental I_B/I_A value for H^+ on Sr (0.35), p is determined as 0.26. If we notice the O peak in Fig. 1(a), elastic peak A is smaller than loss peak B in intensity (though not clearly separated), suggesting the larger neutralization probability in H^+-O collision than in H^+-Sr collision. This is reasonable if one considers the fact that the valence electrons are spatially localized in the oxygen atom.

The intensity of the Sr peak (peak A) in He^+ scattering is almost one order of magnitude smaller than that in H^+ scattering [see Figs. 1(a) and 2(a)]. This is caused by the following factors: (i) The velocity of H^+ is twice as large as He^+, so that T is shorter for H^+ than for He^+. (ii) The hybridization of He 1s with Sr 4p leads to QRN of He^+. (iii) The crossing of the antibonding MO with the valence band results in CIN of He^+.

B. N^+, O^+, and Ne^+

The MO energy of O^+ interacting with the $(SrO_5)^{8-}$ cluster is calculated, and the results are shown in Fig. 11

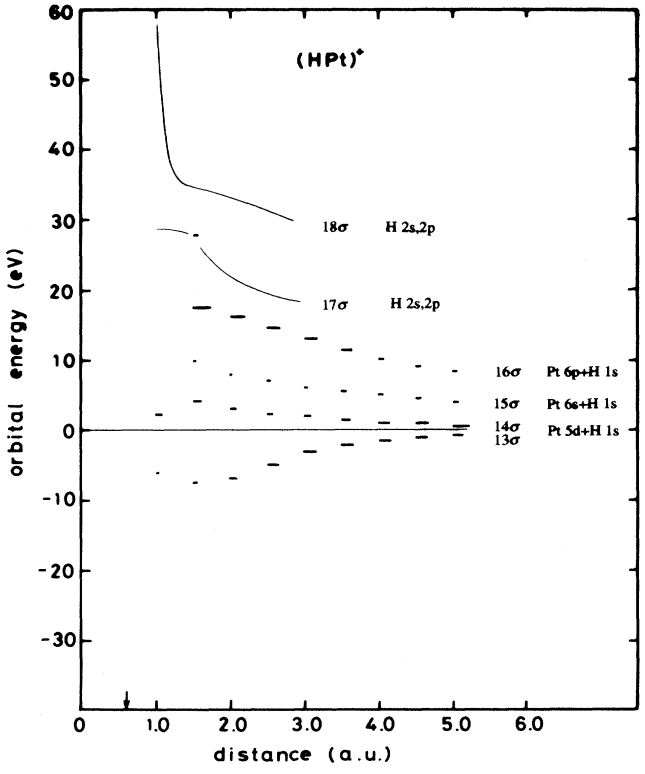

FIG. 9. The energy-level diagram for the $(HPt)^+$ molecule simulating H^+ scattering from Pt of the Pt(111) surface. The energy position and population of the H 1s component in the σ orbital are indicated by the horizontal bars.

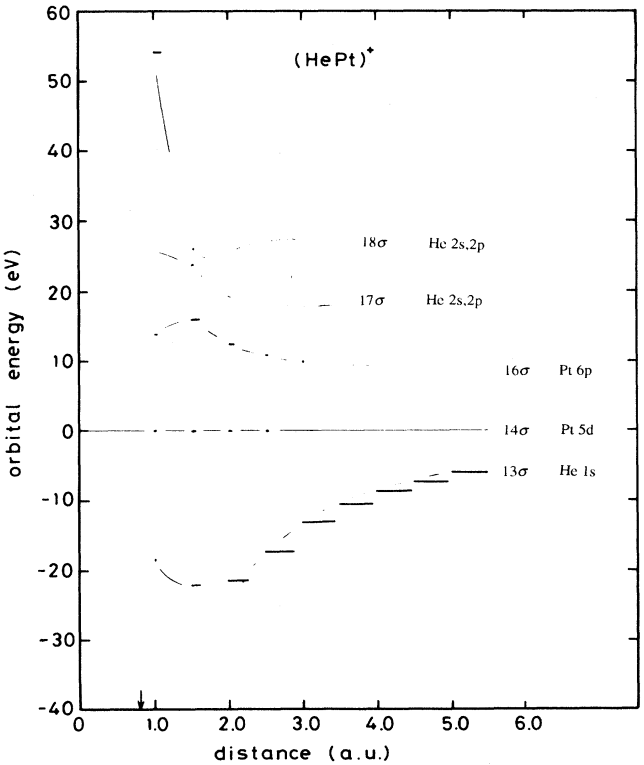

FIG. 10. Same as Fig. 9, but for the $(HePt)^+$ molecule. The energy position and population of the He 1s component in the σ orbital are indicated by the horizontal bars.

for (a) the a_1 orbitals and (b) the e orbitals. The $2s$ and $2p$ orbitals of oxygen are hybridized with the a_1 orbital, while only the O $2p$ orbital contributes to the e orbital. The population of the O $2s$ and $2p$ component in the MO is indicated by the length of the horizontal bar as a function of the distance. As for the a_1 orbitals, the O $2s$ component emerges in the $11a_1$, $12a_1$, and $14a_1$ orbitals,

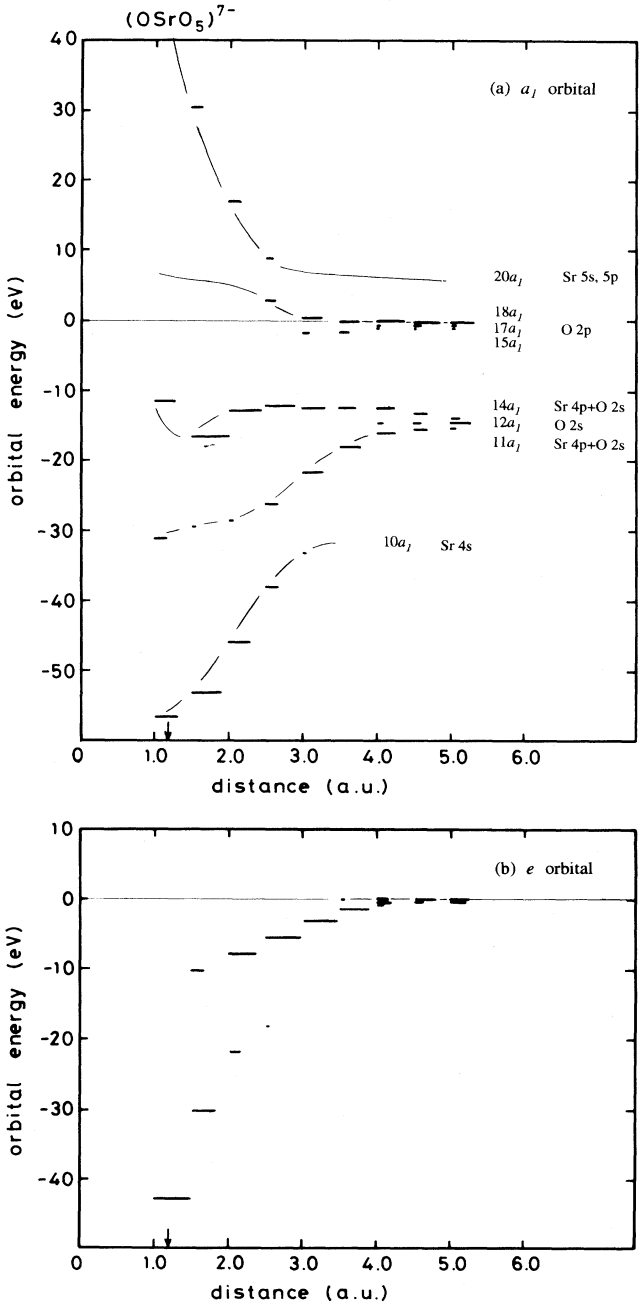

FIG. 11. The energy-level diagram for the $(OSrO_5)^{7-}$ cluster simulating O^+ scattering from Sr^{2+} of the $SrTiO_3(001)$ surface. The energy position and population of the O $2s$ and $2p$ components in the a_1 orbital and the O $2p$ component in the e orbital are plotted as a function of the distance.

whereas the O $2p$ orbital is hybridized with the valence states ($15-18a_1$). With a decrease of the separation, the O $2p$ character is promoted diabatically along the antibonding $18-20a_1$ orbitals. This behavior is very similar to the H $1s$ component distributed in the $16-20a_1$ orbitals shown in Fig. 7. The $11a_1$ and $14a_1$ orbitals in Fig. 11 are the bonding and antibonding MO's formed by hybridization of the O $2s$ and Sr $4p$ orbitals. This is also comparable to the $10a_1$ and $13a_1$ orbitals in He^+ scattering shown in Fig. 8, where the He $1s$ and Sr $4p$ orbitals are hybridized. Despite the similarity, however, the crossing of the $14a_1$ orbital with the valence orbitals ($15-20a_1$) is not sufficient in Fig. 11, so that excitation neither of the O $2s$ electron nor the Sr $4p$ electron is likely to occur from this diagram. The O $2p$ component in the e orbital is distributed mainly around the valence-band state and shifted downwards for a small separation, which causes RN as well as AN but no electronic excitation. The energy loss of the Sr peaks seen in Figs. 3(a) and 4(a) can thus be ascribed to the valence-electron excitation.

The energies of the a_1 orbitals and the e orbitals for Ne^+ on $(SrO_5)^{8-}$ are shown in Fig. 12. At a large separation, the $10a_1$ and $15a_1$ orbitals are dominated by the Ne $2s$ and $2p$ characters, respectively. The Ne $2p$ and Sr $4p$ orbitals, located closely to each other, are hybridized to form the bonding ($12a_1$) and antibonding ($15a_1$) orbitals at moderate separations. The $15a_1$ orbital is promoted sufficiently, and crosses the valence-band states at $d=2.0$ a.u., suggesting the occurrence of electronic excitation similar to the He-Sr collision. In reality, however, the Sr peak shown in Fig. 5(a) is rather simple in structure compared to that shown in Fig. 2(a), and a small energy-loss peak appears. This peak is attributable to excitation of the Ne $2p$ electron rather than the Sr $4p$ electron as described below.

It should be noted that the antibonding $15a_1$ orbital shown in Fig. 12 changes its character as a function of the distance. At a larger distance, the $15a_1$ orbital is dominated by the Ne $2p$ component, and Sr $4p$ is concentrated on the $12a_1$ orbital. In this energy-level configuration, excitation of the Ne $2p$ electron rather than the Sr $4p$ electron is more likely to occur along the $15a_1$ orbital. This provides a sharp contrast to the He^+-Sr collision shown in Fig. 8, where He $1s$ and Sr $4p$ are hybridized significantly relative to each other. Thus the key ingredient leading to such difference is suggested to be the mutual energy separations between the projectile ionic level and the corresponding semicore level of the target. An electronic state shallower than the Ne $2s$ and $2p$ (or He $1s$) levels can basically be excited, provided that sufficient promotion of the diabatic MO occurs. The validity of this criterion is also derived from a large number of experimental results.[18]

The energy-loss peak in Fig. 5(a), therefore, may be caused by reionization of Ne ($Ne^+ \rightarrow Ne^0 \rightarrow Ne^+$). The above discussions may not exclude the occurrence of the valence-electron excitation [corresponding to peak B in Figs. 1(a) and 2(a)], but it is not discernible from the elastic peak. Probably the impact of heavier projectiles may

lead to a broadening of each component peak, which makes the peak separation difficult.

The MO energies for O^+ on Pt are shown in Fig. 13. The O 2*s* orbital is concentrated on 14σ and no strong hybridization occurs with the Pt 5*d* and 6*s* states. The O 2*p* component, on the other hand, appears around the HOMO position for both σ and π orbitals, satisfying the RN condition in energy with the valence-band state. With a decrease of the separation, the O 2*p* character in the σ orbital is partitioned into the bonding 15σ orbital and the antibonding $16-18\sigma$ orbitals. Very few states of oxygen are distributed around the valence-band orbitals for $d < 2.0$ a.u.

The calculated results for $(NePt)^+$ are shown in Fig.

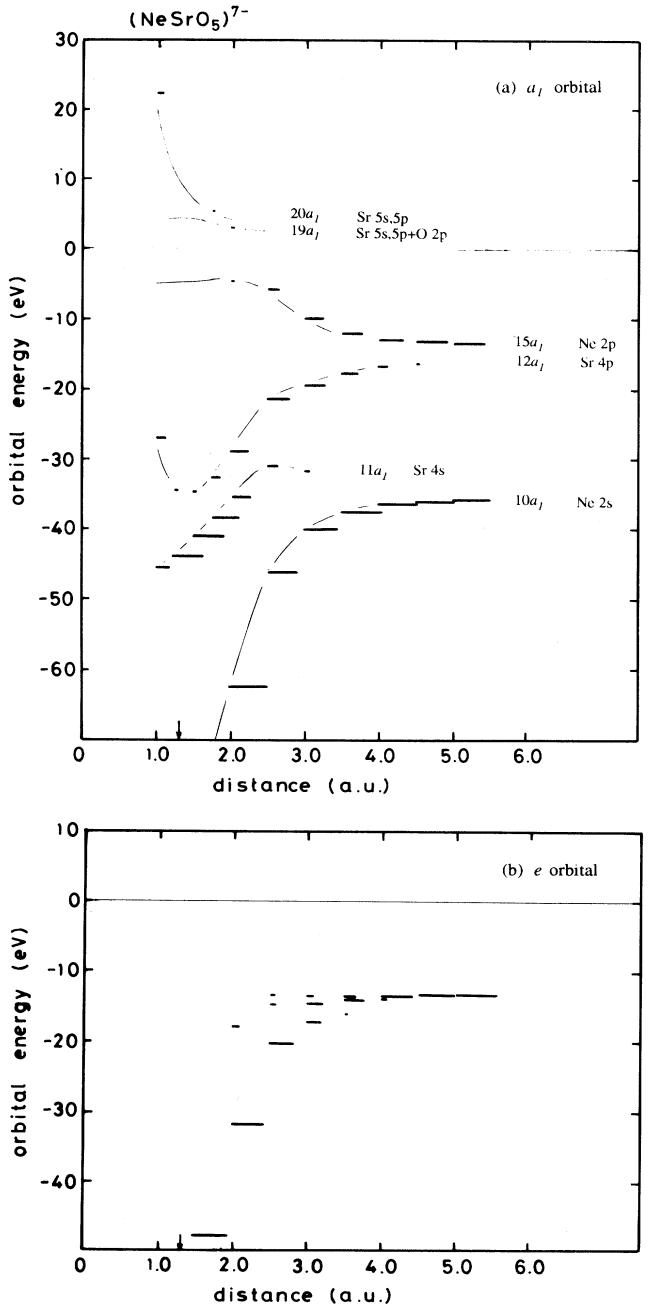

FIG. 12. Same as Fig. 11, but for the $(NeSrO_5)^{7-}$ cluster. The energy position and population of the Ne 2*s* and 2*p* components in the a_1 orbital and the Ne 2*p* component in the *e* orbital are plotted as a function of the distance.

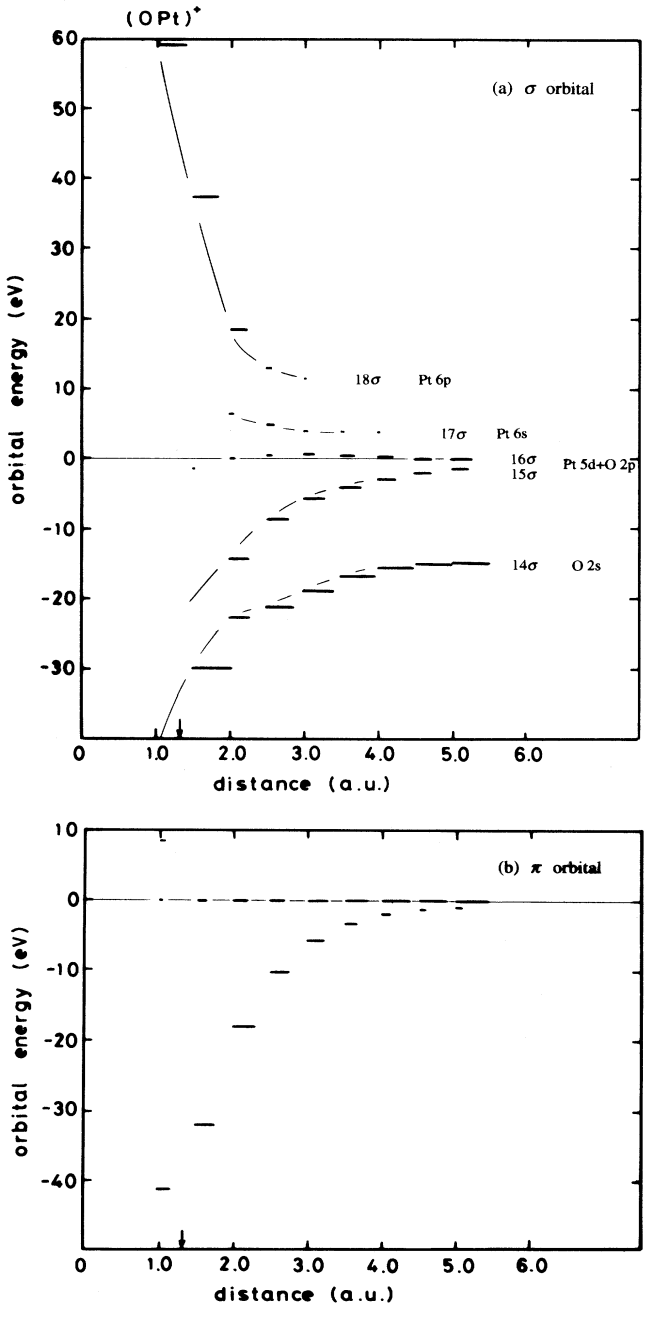

FIG. 13. The energy-level diagram for the $(OPt)^+$ molecule simulating O^+ scattering from Pt of the Pt(111) surface. The energy position and population of the O 2*s* and 2*p* components in the σ orbital and the O 2*p* component in the π orbital are plotted as a function of the distance.

14. The 14σ and 15σ orbitals are composed of Ne $2s$ and $2p$ characters, respectively. The absence of the Ne $2p$ component around the valence-band orbitals indicates that the AN process is responsible for the neutralization of Ne^+. In a close encounter, the 14σ and 15σ orbitals have basically a bonding character with no diabatic correlation with the $16-18\sigma$ orbitals. Hence the Ne $2s$ and $2p$ electrons remain in the adiabatic MO (14σ and 15σ) during collision, and no electronic excitation is mediated by MO's.

MO energies are calculated for C^+ and N^+ ions interacting with $(SrO_5)^{8-}$ and Pt as well. The results are similar to those for O^+ incidence explicitly shown here. For these projectiles, the valence electron is captured via RN, since the $2p$ orbital of the projectile ions is hybridized with the σ and π (a_1 and e) orbitals of the valence-

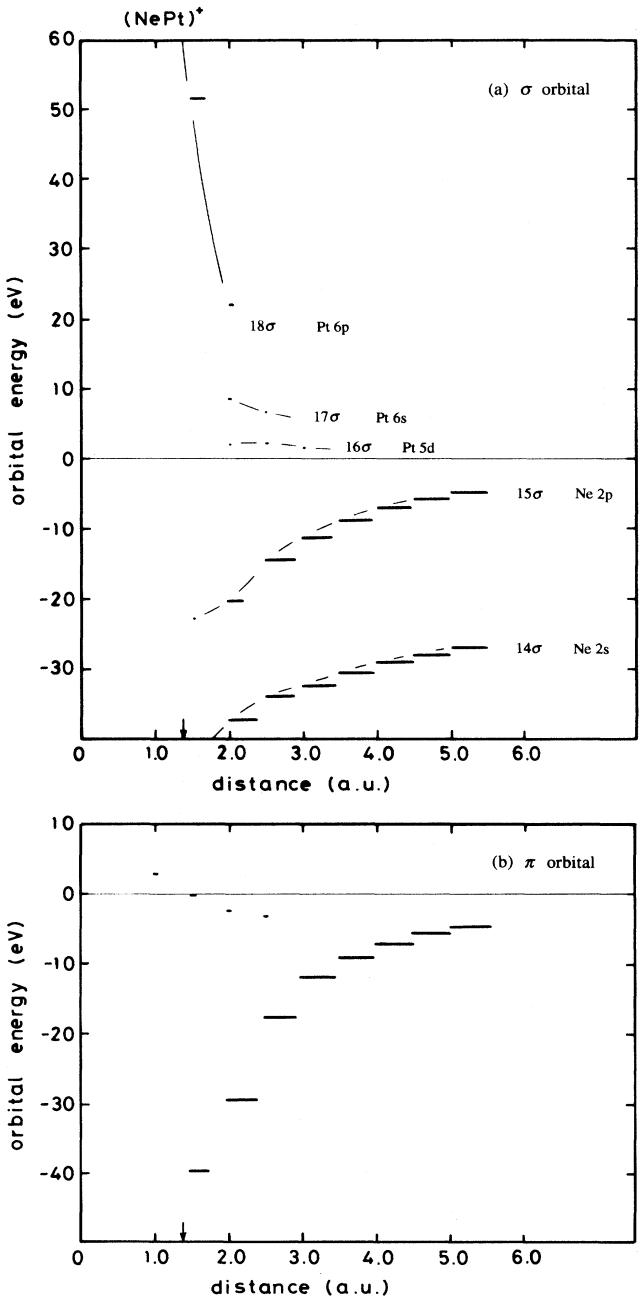

FIG. 14. Same as Fig. 13, but for the $(NePt)^+$ molecule simulating Ne^+ scattering from Pt of the Pt(111) surface. The energy position and population of the Ne $2s$ and $2p$ components in the σ orbital and the Ne $2p$ component in the π orbital are plotted as a function of the distance.

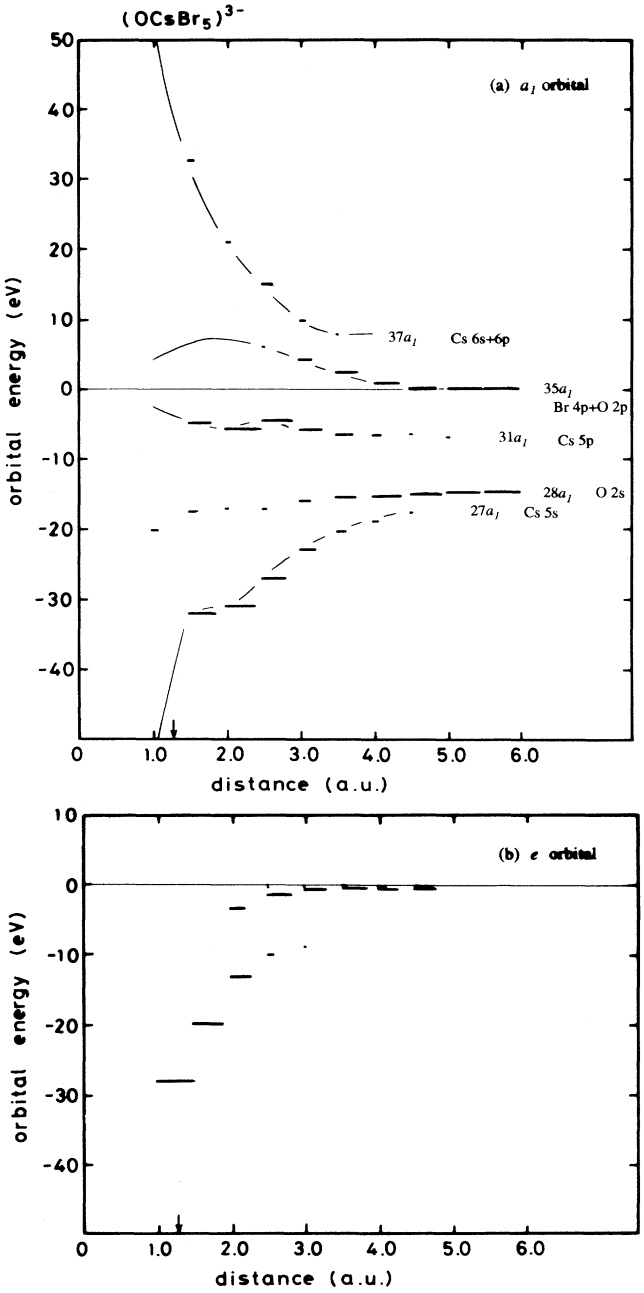

FIG. 15. The energy-level diagram for the $(OCsBr_5)^{3-}$ cluster simulating O^+ scattering from Cs^+ of the CsBr(001) surface. The energy position and population of the O $2s$ and $2p$ components in the a_1 orbital and the O $2p$ component in the e orbital are plotted as a function of the distance.

band states, which is caused essentially by the open-shell structure of the $2p$ orbitals. The fact that the Pt peak in N^+ and O^+ scattering is largely suppressed in intensity relative to the Sr peak is attributed to the band effect of RN, similar to that described for H^+ scattering.

The Sr peak intensity in O^+ scattering is smaller by a factor of 5 than in Ne^+ scattering, which is in apparent contrast to H^+ scattering relative to He^+ scattering, where the Sr peak intensity is much more remarkable in H^+ scattering. Probably this is caused by the small velocity of O^+, by which the RN probability is enhanced relative to H^+. The other possibility is that the $2p$ orbital of O^+ is hybridized not only with the a_1 (σ) orbital but also with the e (π) orbital. The degeneracy of the e (π) orbital is twice as large as the a_1 (σ) orbital, so that the e (π) orbital should play an important role in the charge-exchange behavior. Probably the fact that elastic peak A is absent in O^+ and N^+ scattering, while it is remarkable in H^+ scattering, is related to the additional contribution from the e (π) orbital.

As mentioned above, the Sr peak disappears in the energy spectra of N^+ and O^+ when E_0 is decreased below 200 eV. However, the situation is apparently different in N^+ and O^+ scattering from Cs of CsBr, where the intensity of peak A remains if the beam energy is decreased. Presumably, this is because the RN probability is smaller at CsBr than at $SrTiO_3$, as inferred from the smaller valence-band width of CsBr.

One of the interesting findings in O^+ scattering from CsBr is that the spectral structure changes dramatically at around $E_0=200$ eV. The MO energy diagram for $(OCsBr_5)^{3-}$ is shown in Fig. 15. The promotion of the antibonding $35-37a_1$ orbitals induces electronic excitation, whereas the e orbital causes RN and AN. The existence of the critical energy for the appearance of peak B arises from an energy-level crossing point in the MO energy diagram, which in this case may occur between $35a_1$ and $37a_1$ orbitals at $d=2.5-3.0$ a.u. The distance of 2.5 a.u. (3.0 a.u.) can be reached by $E_0=40$-eV ($E_0=15$-eV) O^+ ions. This value is reasonable since peak B, though small, remains in the $E_0=100$-eV spectrum of O^+ shown in Fig. 6(d). However, the calculated energy does not correspond to the experimental energy of $200\sim250$ eV, where the intensity of peak B begins to increase dramatically. According to the Landau–Zener model,[12] the probability that the electron remains in the same adiabatic MO after crossing is given as

$$P=\exp[-2\pi V^2/\hbar v\Delta F] , \quad (3)$$

where V is the interaction matrix element, ΔF is the difference in slope of the two potential surfaces, and v is the relative velocity of the collision. Probably, the slow velocity of the O^+ ion or the gentle slope of the $35a_1$ orbital may keep adiabaticity to some extent at the crossing point between the $35a_1$ and $37a_1$ orbitals, resulting in the delay of the dramatic increase of the peak B intensity.

V. CONCLUSION

The electronic transition in low-energy ion scattering from metal and ionic-compound surfaces has been discussed from a combination of the experiments and the molecular-orbital energy calculations. The rare-gas ions (He^+, Ne^+) capture a valence electron mainly via the Auger neutralization process, whereas the resonant tunneling process plays an important role in neutralization of the reactive ions (H^+, N^+, O^+). It is concluded that the open-shell structure of the reactive ions causes orbital hybridization with the valence-band state, by which the valence electron can be captured via the resonant-tunneling process. At the Pt(111) surface, the reactive ions are neutralized with a larger probability than the rare-gas ions because resonance neutralization is a much more efficient process than Auger neutralization. The reactive ions are readily equilibrated at the metal surface, and form neutral products because of the large electron mobility in the valence band (band effect). At ionic-crystal surfaces such as $SrTiO_3(001)$ and CsBr, on the other hand, the small electron mobility as inferred from the narrow valence-band width avoids complete neutralization of the reactive ions during the limited collision time (10^{-15} sec) and, hence, the ions survive neutralization to some extent. The excitation of the surface electron occurs due to the electron promotion mechanism. As for the reactive ions, the shallowest valence electron can be excited during scattering as a consequence of the neutralization/ionization sequence along the promoted diabatic molecular orbital. On the other hand, the He $1s$ and Ne $2s$ and $2p$ orbitals can hybridize with semicore orbitals of the target atoms, so that a remarkable target-element dependence emerges in electronic excitation as well as in ion neutralization. The promotion of the antibonding molecular orbitals is an essential prerequisite for the occurrence of electronic excitation, by which target electronic states energetically shallower than the ionic level of the rare-gas projectiles can be excited.

ACKNOWLEDGMENT

We are indebted to Professor H. Adachi of Kyoto University for use of the DV-$X\alpha$ calculation program.

[1]H. D. Hagstrum, Phys. Rev. **96**, 336 (1954).
[2]R. Souda and M. Aono, Nucl. Instrum. Methods B **15**, 114 (1986).
[3]J. W. Rabarais, J. N. Chen, and R. Kumar, Phys. Rev. Lett. **55**, 1124 (1985); G. Zampieri, F. Meier, and R. Baragiola, Phys. Rev. A **29**, 116 (1984).
[4]M. Barat and W. Lichten, Phys. Rev. A **6**, 211 (1972).
[5]S. Tsuneyuki and M. Tsukada, Phys. Rev. B **34**, 5758 (1986).
[6]W. Eckstein, in *Inelastic Particle-Surface Collisions,* edited by E. Taglauer and W. Heiland, Springer Series in Chemical Physics Vol. 7 (Springer, New York, 1981), p. 157.
[7]R. Souda, T. Aizawa, W. Hayami, S. Otani, and Y. Ishizawa, Phys. Rev. B **42**, 7761 (1990); **50**, 1934 (1994); **50**, 4733 (1994).
[8]R. Souda, W. Hayami, T. Aizawa, S. Otani, and Y. Ishizawa,

Phys. Rev. Lett. **69**, 192 (1992); R. Souda, Int. J. Mod. Phys. B **8**, 679 (1994).
[9]R. Souda, K. Yamamoto, W. Hayami, B. Tilley, T. Aizawa, and Y. Ishizawa, Phys. Rev. B **50**, 18 849 (1994).
[10]H. D. Hagsrum, P. Petrie, and E. E. Chaban, Phys. Rev. B **38**, 10 264 (1988).
[11]H. Muller, R. Hausmann, H. Brenten, and V. Kempter, Surf. Sci. **284**, 129 (1993); **291**, 78 (1993); **303**, 56 (1994); H. Muller, G. Gador, H. Brenten, and V. Kempter, *ibid.* **313**, 188 (1994).
[12]S. Tsuneyuki, N. Shima, and M. Tsukada, Surf. Sci. **186**, 26 (1987).
[13]H. Adachi, M. Tsukada, and C. Satoko, J. Phys. Soc. Jpn. **45**, 875 (1978).
[14]C. Satoko, M. Tsukada, and H. Adachi, J. Phys. Soc. Jpn. **45**, 1333 (1978).
[15]R. L. Erickson and D. P. Smith, Phys. Rev. Lett. **34**, 297 (1975).
[16]A. Zartner, E. Taglauer, and W. Heiland, Phys. Rev. Lett. **40**, 1259 (1978).
[17]J. C. Tully, Phys. Rev. B **16**, 4324 (1977).
[18]R. Souda, T. Aizawa, C. Oshima, S. Otani, and Y. Ishizawa, Phys. Rev. B **40**, 4119 (1989).
[19]R. Souda, T. Aizawa, C. Oshima, and Y. Ishizawa, Nucl. Instrum. Methods B **45**, 364 (1990).